Structural Engineering and Mechanics, Vol. 18, No. 2 (2004) 167-194
DOI: http://dx.doi.org/10.12989/sem.2004.18.2.167

Low strength concrete members externally confined with FRP sheets

Alper Ilki†, Nahit Kumbasar‡ and Volkan Koc‡†

Istanbul Technical University, Civil Engineering Faculty, 34469, Maslak, Istanbul, Turkey

(Received September 15, 2003, Accepted March 8, 2004)

Abstract. In this paper axial loading tests on low strength concrete members, which were confined with various thickness of carbon fiber reinforced polymer (CFRP) composite sheets are described. Totally 46 specimens with circular, square and rectangular cross-sections with unconfined concrete compressive strengths between 6 and 10 MPa were included in the test program. During the tests, a photogrammetrical deformation measurement technique was also used, as well as conventional measurement techniques. The contribution of external confinement with CFRP composite sheets to the compressive behavior of the specimens with low strength concrete is evaluated quantitatively, in terms of strength, longitudinal and lateral deformability and energy dissipation. The effects of width/depth ratios and the corner radius of the specimens with rectangular cross-section on the axial behavior were also examined. It was seen that the effectiveness of the external confinement with CFRP composite sheets is much more pronounced, when the unconfined concrete compressive strength is relatively lower. It was also found that the available analytical expressions proposed for normal or high strength concrete confined by CFRP sheets could not predict the strength and deformability of CFRP confined low strength concrete accurately. New expressions are proposed for the compressive strength and the ultimate axial strain of CFRP confined low strength concrete.

Key words: compression; concrete; confined concrete; ductility; fibers; stress-strain curves.

1. Introduction

In many developing countries all around the world, there are a huge number of existing buildings, which suffer from various design and construction deficiencies. Low quality of concrete and lack of adequate confinement reinforcement are between the most common deficiencies. These structural deficiencies may cause significant increase of damage during earthquakes in seismic areas. To avoid damage, axial load capacity and the deformability of such vertical structural members may need to be enhanced to exhibit satisfactory seismic performance. External confinement of this type of structural members with high strength fiber reinforced polymer (FRP) composite sheets can enhance the axial strength and deformability of the members significantly. Compared to conventional retrofitting techniques, lower density, higher tensile strength and modulus, durability and good constructional workability are the advantages of the composite retrofitting system. Particularly, when

† Assistant Professor, Structural and Earthquake Engineering Laboratory
‡ Professor, Reinforced Concrete Division
‡† Research Fellow

there is a time limitation for retrofit procedure and/or access to the members to be strengthened is limited, composite retrofitting system may be more preferable. Due to these advantages, the use of FRP composites in civil engineering structures has been increasing rapidly in recent years.

In this study, low strength concrete specimens with different cross-sections were tested under concentric compression. The test program includes 14 cylinders, 8 specimens with square cross-section and 24 specimens with rectangular cross-section having depth/width ratios of 1.5, 2 and 3. The standard unconfined concrete cylinder compressive strength was between 6 and 10 MPa for these specimens. The specimens were either unconfined or jacketed by 1, 3 or 5 plies of CFRP composite sheets for rectangular specimens, and by 1, 2, 3, 4, 5 and 6 plies for cylinders in sets of two. The experimental results showed that the efficiency of the CFRP jackets on strength and ductility enhancement of low strength concrete is higher than that of normal or high strength concrete both for specimens with circular and non-circular cross-sections. Consequently, equivalent ductility or strength enhancement can be obtained with relatively smaller jacket thickness resulting with more economical retrofit design. The experimental results on similar specimens that have higher concrete compressive strength (around 30 MPa) can be found elsewhere (Ilki and Kumbasar 2003). It should be noted that the average characteristic concrete compressive strength in various cities of Turkey was determined to be around 10 MPa (Igarashi 1999).

Photogrammetric deformation measurements were also carried out as well as conventional deformation and displacement measurements carried out by using strain gages and displacement transducers. With the help of the photogrammetric measurements, deformation characteristics of the specimens could be analyzed in more detail. When compared to deformation measurements with strain gages, photogrammetric deformation measurements have further advantages like; availability of all surface deformations in three dimensions, comparable precision, lower cost, convenience of test setup installation in a short time and practically unlimited deformation capacity. The deformation patterns obtained by the photogrammetric measurements are generally in good agreement with the deformations determined by the conventional techniques. Consequently, the photogrammetric measurement technique seems to be promising as an alternative or additional way of conventional deformation measurements.

Analytical expressions that were proposed for the compressive strength and ultimate axial strain of FRP composite sheet wrapped normal or high strength concrete were not accurate in the case of low strength concrete. So, based on the experimental data, new expressions are proposed for the strength and strain capacities of low strength concrete members externally confined with FRP composite sheets, as well as a bilinear stress-strain relationship with a curved transition.

It is important to note that the experimental work and derived conclusions are based on the testing of relatively small size specimens. Consequently, the validity of these results may need to be verified for actual size reinforced concrete members.

2. Research significance

Almost all of the experimental and analytical research work on FRP jacketed concrete was carried out on specimens with normal or high concrete compressive strength. However, there are many existing structures, those were not designed or built considering the up-to-date codes and recommendations. Consequently, these structures may experience severe damages due to insufficient ductility and low concrete compressive strength during earthquakes. Although demolition of such poor structures may be necessary, considering the huge number of existing buildings in this condition, demolition of all of these structures is practically impossible. External confinement of vertical structural members of this type of structures with high strength FRP composite sheets can enhance the axial strength and deformability of the members significantly. Therefore, there is a need of research on the behavior of low strength concrete jacketed with FRP composite sheets.

In addition, a great majority of the experimental data on FRP confined concrete is on small size cylinder specimens. For a better understanding of the behavior of the FRP jacketed concrete members with rectangular cross-sections, more experimental work examining the effects of various parameters on the behavior is needed. This paper attempts to provide experimental data on FRP jacketed low strength concrete members with different cross-sectional shapes and dimensions.

3. Previous research

Various experimental and analytical studies proved that significant enhancement in compressive strength and deformability of concrete is possible by adequate confinement of concrete with lateral reinforcement (Kent and Park 1971, Priestley *et al.* 1981, Park *et al*. 1982, Sheikh and Uzumeri 1982, Mugurama *et al*. 1983, Ahmad and Shah 1985, Mander *et al*. 1988a, 1988b, Mugurama and Watanabe 1990, Saatcioglu and Razvi 1992, Saatcioglu *et al.* 1995, Hoshikuma *et al.* 1997, Ilki *et al.* 1997).

External confinement of concrete with high strength FRP composites can also provide similar enhancement on the behavior of concrete. According to Fukuyama and Sugano (2000) the repair and seismic strengthening by continuous fiber sheet wrapping method was first developed in Japan, whose research was first carried out in 1979. They presented an outline of the continuous fiber wrapping technique by comparing experimental data obtained for various rehabilitation techniques with a special emphasis on performance based engineering and effective rehabilitation techniques without hindrance of building operation. Fardis and Khalili (1982) stated that, excellent strength and ductility characteristics were obtained during the experimental study on the FRP encased concrete cylinders in axial compression and of rectangular FRP encased beams in bending. The studies of Harmon and Slattery (1992), Demers and Neale (1994), and Nanni and Bradford (1995) are among the initial experimental works on confinement of concrete members with FRP composites. Saadatmanesh *et al.* (1994), examined the behavior of concrete columns externally reinforced with fiber composite straps and proposed an analytical model to quantify the gain in strength and ductility by adopting the confined concrete stress-strain model proposed by Mander *et al.* (1988b) to the fiber composite straps case. Fyfe (1996) and Guadagnini *et al.* (2001) summarized the going on research on FRP composites, in United States and Europe, respectively. Mirmiran and Shahawy (1997), reported that, the available models in literature that were originally developed for conventional reinforced concrete columns generally did not give accurate results for FRP wrapped concrete members. Karbhari and Gao (1997) developed experimental data for cylinder specimens, based on a variety of fiber types, orientations and jacket thickness. Toutanji (1999) investigated the effect of type of wrapping material on the behavior of FRP jacketed concrete cylinder specimens. Saafi *et al.* (1999), Fam and Rizkalla (2001) and Becque *et al.* (2003) investigated the behavior of concrete filled FRP tubes under uniaxial compressive load. Saafi *et al.* (1999) indicated that the available models generally overestimate the strength of concrete confined by FRP tubes, resulting in unsafe design. Spoelstra and Monti (1999), proposed a uniaxial model, which can be used both for concrete confined with FRP composites and conventional transverse reinforcement. Rochette and Labossiere (2000) conducted axial loading tests on FRP jacketed specimens with circular, square and rectangular cross-section. They analyzed the effect of corner radius on the behavior of specimens with non-circular cross-sections. Wang *et al.* (2000), and Wang and Restrepo (2001), tested square and rectangular concrete columns confined by glass fiber composites. In their study, Mander's model (1988b) is adopted for the stress-strain behavior of FRP wrapped concrete. Xiao and Wu (2000) investigated the effect of concrete compressive strength and thickness of CFRP jacket wrapped around cylinder specimens. They also proposed a simple bilinear stress-strain model for CFRP jacketed concrete. Tan (2002) tested half scale reinforced concrete rectangular columns with a section aspect ratio of 3.65 under axial loads and investigated the effects of fiber type and configuration and fiber anchors on the strength enhancement of the columns. Ilki and Kumbasar (2002) tested both damaged and undamaged cylinder specimens, which were externally confined with different thickness of CFRP jackets, under monotonic increasing and repeated compressive stresses. Based on experimental results they proposed simple expressions for ultimate strength and corresponding axial strain of CFRP wrapped concrete. Maalej *et al.* (2003), tested rectangular reinforced concrete columns and proposed a load-displacement model, which took into account the lateral confining pressure from the transverse reinforcement as well as the FRP wraps. Lam and Teng (2002) carried out an extensive survey of existing studies on FRP confined concrete and proposed a simple model based on the linear relationship between confined concrete strength and lateral confining pressure provided by FRP composites, which was quite similar to the model proposed by Ilki and Kumbasar (2002) before. They also studied the compressive behavior of FRP confined concrete in elliptical columns, (Teng and Lam 2002). Ilki and Kumbasar (2003), after testing CFRP wrapped concrete specimens with square and rectangular cross-sections, modified the expressions that they have proposed before to cover non-circular cross-sections. Campione and Miraglia (2003) also examined the behavior of concrete members of different shape of transverse cross-section confined with FRP composite sheets, and proposed a stress-strain model. Chaallal *et al.* (2003) examined the effects of the concrete strength, aspect ratio of the cross-section and number of FRP layers on the axial behavior of small size short rectangular columns. Lam and Teng (2003a, 2003b) proposed design oriented stress-strain models for both uniformly and non-uniformly confined concrete members.

Despite extensive experimental and analytical work carried out in recent years, the behavior of FRP confined concrete still needs to be investigated for determining the effects of different parameters. Even for the case of FRP confined cylinders, which is much more simple than the case of FRP confined rectangular concrete members, in a recent comparative study by De Lorenzis and Tepfers (2003), it was stated that none of the available models could predict the strain at peak stress with reasonable accuracy.

4. Test program

The research program involved the construction and testing of 14 cylinders, 8 specimens with square cross-section and 24 specimens with rectangular cross-section having depth/width ratios of 1.5, 2 and 3. The dimensions of the specimens are presented in Fig. 1. As well as unconfined specimens, specimens externally confined with various thicknesses of CFRP jackets were tested under concentric compression. The test parameters were the thickness of the external confinement

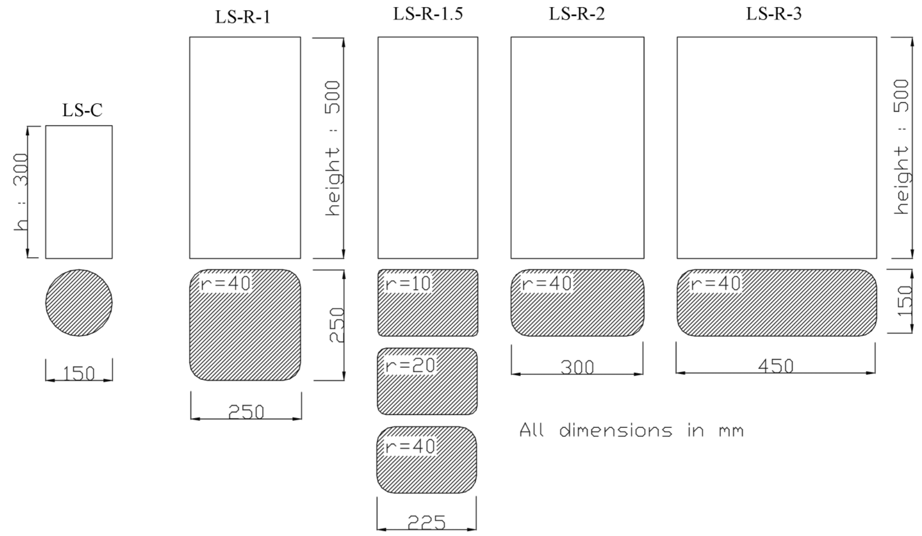

Fig. 1 Dimensions of the specimens

Table 1 Concrete mix-proportions and standard cylinder strengths at 28 days

Batch (1)	Cement (kg/m^3) (2)	Water (kg/m^3) (3)	Sand (kg/m^3) (4)	Gravel (kg/m^3) (5)	f'_c (MPa) (6)
1	150	191	932	1074	6.2
2	160	191	932	1074	10.5

jacket, the shape of the cross-section and the corner radius for specimens with rectangular cross-section. Specially designed ready mixed concrete was used for all specimens for obtaining low concrete strength. Standard cylinder compression tests were carried out at the ages of 28, 90 and 180 days. The concrete mix-proportions and 28 days standard cylinder compressive strengths (f_c') are presented in Table 1. In the mixture ordinary Portland cement with the 28 days strength of 42.5 MPa was used. The maximum aggregate size was 10 mm. The specimens did not have any longitudinal and transverse steel reinforcement. It should be noted that Demers and Neale (1999) stated that for the cases of stirrup spacings medium to large, tests on plain concrete specimens are sufficient for investigation of this retrofit method, as the key parameters, which really affect strength and ductility are the concrete strength, composite fiber type and sheet thickness.

Except the specimens those were tested without external confinement, all the specimens were jacketed externally by unidirectional CFRP sheets in transverse direction with 0-degree orientation. Before wrapping the specimens with CFRP jackets, surface preparation procedure was carried out, which included sanding, cleaning, forming one layer of epoxy-polyamine primer and one layer of epoxy putty. Then epoxy adhesive was used for bonding CFRP jacket on the specimens. Additional layers of epoxy adhesive were applied between the CFRP jacket plies and on the outer ply of CFRP jacket when more than one ply was wrapped. The compressive and tensile strengths of the epoxy system were around 80 and 50 MPa, respectively. Tensile elasticity modulus of the epoxy system was around 3000 MPa and its ultimate elongation was 0.025. The steps during jacketing need to be carried out with great care to prevent stress concentrations due to surface irregularities and to obtain the tight fitting of the CFRP jackets on the specimens. For obtaining satisfactory bonding, 150 mm overlap length was considered at the end of the wrap. In the cases of wrapped sheets to be more than one ply, the sheet was wrapped continuously and 150 mm overlap was formed at the end of the wrap. The mechanical and geometrical properties of the CFRP sheets are given in Table 2. These properties are taken from the specifications of the manufacturer (Mbrace 2000).

The details of the specimens with circular and rectangular cross-sections are presented in Tables 3 and 4, respectively. In these tables, experimentally determined compressive strengths, the ultimate axial strains and the maximum measured transverse strains are also presented. In these tables, f'_{co} and ε_{co} are the unconfined concrete strength and corresponding axial strain, f'_{cc} and ε_{cc} are the confined concrete strength and ultimate axial strain, ε_{ch} is the maximum measured transverse strain, and r is the corner radius. The specimen names are assigned considering the shape and depth/width ratio of the cross-section, number of transverse CFRP plies and the corner radius. As an example LS-R-1-3-40a represents the specimen with **R**ectangular cross-section of depth/width ratio **1**, which is wrapped by **3** plies of transverse CFRP sheets. The corner radius of this specimen is **40** mm. The first two characters, **LS** stand for low strength concrete.

Table 2 The mechanical and geometrical properties of CFRP sheets

Characteristic Tensile Strength (MPa) (1)	Characteristic Tensile Modulus (MPa) (2)	Maximum Tensile Strain (mm/mm) (3)	Effective Area Per Unit Width (mm^2/mm) (4)	Unit Weight (kg/m^3) (5)
3430	230000	0.015	0.165	1820

Table 3 The details and test results of the specimens with circular cross-section

Specimen (1)	Batch (2)	f'_{co} (MPa) (3)	Plies (4)	f'_{cc} (MPa) (5)	ε_{co} (6)	ε_{cc} (7)	ε_{ch} (8)	f'_{cc}/f'_{co} (9)	$\varepsilon_{cc}/\varepsilon_{co}$ (10)
LS-C-0	1	6.2	0	-	0.002	-	-	-	-
LS-C-1a	1	6.2	1	25.3	0.002	0.039	0.0067	4.08	19.50
LS-C-1b	1	6.2	1	19.4	0.002	0.026	0.0062*	3.13	13.00
LS-C-2a	1	6.2	2	41.9	0.002	0.059	0.0130	6.76	29.50
LS-C-2b	1	6.2	2	40.0	0.002	0.059	0.0053*	6.45	29.50
LS-C-3a	1	6.2	3	52.2	0.002	0.069	0.0072*	8.42	34.50
LS-C-3b	1	6.2	3	56.9	0.002	0.075	0.0110	9.18	37.50
LS-C-4a	1	6.2	4	76.6	0.002	0.085	0.0093*	12.35	42.50
LS-C-4b	1	6.2	4	69.7	0.002	0.076	0.0110*	11.24	38.00
LS-C-5a	1	6.2	5	87.7	0.002	0.091	0.0097*	14.15	45.50
LS-C-5b	1	6.2	5	82.7	0.002	0.094	0.0054*	13.34	47.00
LS-C-6a	1	6.2	6	108.3	0.002	0.104	0.0120*	17.47	52.00
LS-C-6b	1	6.2	6	103.3	0.002	0.096	0.0069*	16.66	48.00

*Strain gages were out of order before peak load.

Table 4 The details and test results of the specimens with square and rectangular cross-section

Specimen	Batch	f'_{co} (MPa)	Plies	r (mm)	f'_{cc} (MPa)	ε_{co}	ε_{cc}	ε_{ch} long side	ε_{ch} short side	f'_{cc}/f'_{co}	$\varepsilon_{cc}/\varepsilon_{co}$
(1)	(2)	(3)	(4)	(5)	(6)	(7)	(8)	(9)	(10)	(11)	(12)
LS-R-1-0-40	1	6.8	0	40	-	0.0028	-	-	-	-	-
LS-R-1-1-40a	1	6.8	1	40	11.1	0.0028	0.039	0.0092	-	1.63	13.93
LS-R-1-1-40b	1	6.8	1	40	11.4	0.0028	0.024	0.0100	-	1.68	8.57
LS-R-1-3-40a	1	6.8	3	40	23.8	0.0028	0.060	0.0120	-	3.50	21.43
LS-R-1-3-40b	1	6.8	3	40	20.1	0.0028	0.046	0.0071*	-	2.96	16.43
LS-R-1-5-40a	1	6.8	5	40	35.8	0.0028	0.088	0.0100	-	5.26	31.43
LS-R-1-5-40b	1	6.8	5	40	36.1	0.0028	0.086	0.0120	-	5.31	30.71
LS-R-1.5-0-10	2	9.5	0	10	-	0.002	-	-	-	-	-
LS-R-1.5-3-10a	2	9.5	3	10	18.6	0.002	0.066	0.0110	0.0120	1.96	33.00
LS-R-1.5-3-10b	2	9.5	3	10	20.2	0.002	0.076	-	-	2.13	38.00
LS-R-1.5-3-20a	2	9.5	3	20	27.1	0.002	0.056	-	-	2.85	28.00
LS-R-1.5-3-20b	2	9.5	3	20	27.3	0.002	0.071	0.0120*	0.0120*	2.87	35.50
LS-R-1.5-3-40a	2	9.5	3	40	37.9	0.002	0.050	-	-	3.99	25.00
LS-R-1.5-3-40b	2	9.5	3	40	36.2	0.002	0.045	0.0092*	0.0100*	3.81	22.50
LS-R-2-0-40	1	7.2	0	40	-	0.0028	-	-	-	-	-
LS-R-2-1-40a	1	7.2	1	40	13.2	0.0028	0.032	0.0110	0.0095	1.83	11.43
LS-R-2-1-40b	1	7.2	1	40	11.5	0.0028	0.023	0.0065	0.0079	1.60	8.21
LS-R-2-3-40a	1	7.2	3	40	23.6	0.0028	0.077	0.0091	0.0084*	3.28	27.50
LS-R-2-3-40b	1	7.2	3	40	21.1	0.0028	0.079	0.0083	0.0087	2.93	28.21
LS-R-2-5-40a	1	7.2	5	40	32.8	0.0028	0.098	0.0110	0.0093	4.56	35.00
LS-R-2-5-40b	1	7.2	5	40	31.3	0.0028	0.099	0.0110	0.0090	4.35	35.36
LS-R-3-0-40	2	9.8	0	40	-	0.0024	-	-	-	-	-
LS-R-3-1-40a	2	9.8	1	40	10.2	0.0024	0.024	-	-	1.04	10.00
LS-R-3-1-40b	2	9.8	1	40	12.0	0.0024	0.031	0.0100	0.0150	1.22	12.92
LS-R-3-3-40a	2	9.8	3	40	15.1	0.0024	0.072	-	-	1.54	30.00
LS-R-3-3-40b	2	9.8	3	40	16.6	0.0024	0.061	0.0094	0.0140	1.69	25.42
LS-R-3-5-40a	2	9.8	5	40	20.1	0.0024	0.098	-	-	2.05	40.83
LS-R-3-5-40b	2	9.8	5	40	17.1	0.0024	0.099	0.0097	0.0130	1.74	41.25

*Strain gages were out of order before peak load.

The cylinder specimens were capped with gypsum mortar before testing. Specimens with rectangular cross-section were not capped because they were cast in horizontal position in the formwork, and both top and bottom surfaces of these specimens were perfectly flat.

4.1 Instrumentation and loading setup

An Amsler universal testing machine with the capacity of 5000 kN was used for applying concentric compressive loads on the specimens. The tests were carried out in a static manner by controlling the axial displacements. The axial and transverse strains were measured at mid-height of the specimens by using surface strain gages with the gage length of 60 mm. For specimens with circular cross-section (150 mm × 300 mm), two vertically and two horizontally bonded strain gages were used with 180 degree intervals around perimeter, for non-circular specimens at least one vertical and one horizontal strain gages were bonded on each side. The locations of the strain gages on the specimens with square and rectangular cross-section are shown in Fig. 2. For measurement of the average axial strains for different gage lengths, displacement transducers were used. For specimens with circular cross-section, two transducers with the gage length of 300 mm were used. For specimens with rectangular cross-section, four transducers with the gage length of 500 mm were used, Fig. 3. As also mentioned by Mirmiran and Shahawy (1997), for determining the overall behavior, the average axial strains measured by the displacement transducers are as accurate as the measurements recorded by the strain gages, consequently in this paper, the given axial strains were obtained by the measurements of the displacement transducers, unless otherwise is mentioned.

As well as conventional measurements, photogrammetric deformation measurements were also carried out for a better understanding of distribution of the axial and transverse strains. In this close range photogrammetric application deformation measurement, analysis, and camera calibration are the most important steps. Twin Industrial Basler A302fs cameras with IEEE 1394 standard were calibrated with 16 mm fix focused Cosmicar Pentax lenses on the test setup. Then, the experimental data capturing system was designed in order to capture the images during tests in which about 20 stereo images were captured periodically. The first image pairs were captured before loading and the exterior orientation parameters were calculated. For deformation analysis, camera stations were fixed all through the test duration in order to use the same orientation parameters for other image pairs. The configuration of the signal points on the specimens was designed so that deformations could be determined by the coordinate differences recorded during loading. The derived exterior orientation parameters were obtained with 0.01 mm and the rotations were obtained with 0.001 radian accuracy.

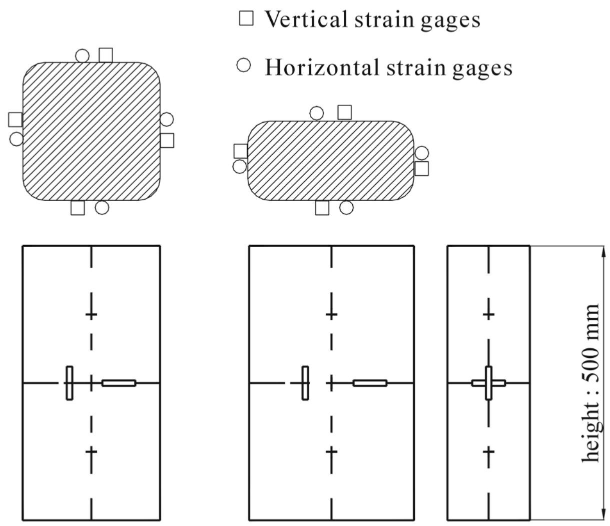

Fig. 2 Locations of the strain gages bonded on the specimens with square and rectangular cross-section

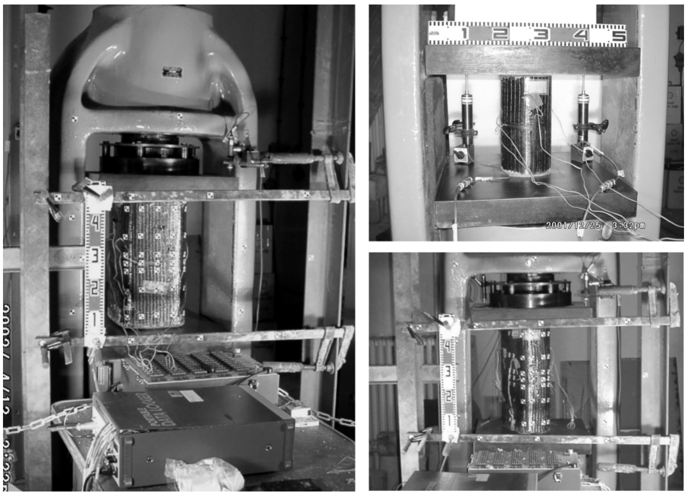

Fig. 3 Test setup for the specimens with square, circular and rectangular cross-section

4.2 Experimental results and observations

The experimental axial stress-axial strain relationships for the specimens with circular cross-section are presented in Fig. 4. The axial stress-axial strain relationships for specimens with rectangular cross-section are given in Figs. 5, 6, 7 and 8 for depth/width ratios of 1, 1.5, 2 and 3, respectively. The axial stress-transverse strain relationships for specimens with circular and square cross-sections are given in Fig. 9, and for specimens with rectangular cross-section of depth/width ratios 1.5, 2 and 3 in Fig. 10. In these relationships σ_c is the axial stress on the specimens at any step of the loading. The transverse strains presented in Figs. 9 and 10 were determined by the strain gage measurements at mid-heights of the specimens. It should be noted that for some of the specimens the strain gages were out of order before ultimate state as also indicated in Tables 3 and 4. The differences between the measured lateral strains of the identical specimens can be attributed to the uneven distribution damage and/or the readability problems of strain gages at large strains due to imperfections of bonding process and their readability capacities.

Failures of all of the specimens were due to sudden tensile failure of CFRP composite sheets at axial strains varying from 0.023 to 0.104. Considering the ultimate axial strain levels for CFRP jacketed normal strength concrete specimens, these values for ultimate axial strains are significantly higher. The enhancement in axial strength is also significantly higher when the unconfined concrete compressive strength is relatively low. Consequently, it is clear that efficiency of CFRP jacketing increases significantly, when the unconfined concrete compressive strength of the jacketed member is low. The comparison of enhancements in compressive strength and ultimate axial strain for low (f'_{co} : 6~7 MPa) and normal strength concrete specimens (f'_{co} : 30~35 MPa), which were wrapped with identical CFRP jackets are presented in Figs. 11, 12 and 13 for specimens with circular, square and rectangular cross-sections (depth/width = 2). In these figures NS and LS represent normal and low strength concrete, respectively. The strength and deformability enhancements of CFRP jacketed normal strength concrete are taken from the study carried out by Ilki and Kumbasar (2003). It should be noted that the loading setup, the measuring system and the boundary conditions were similar for the tests carried out on the specimens with low and normal concrete strength. As

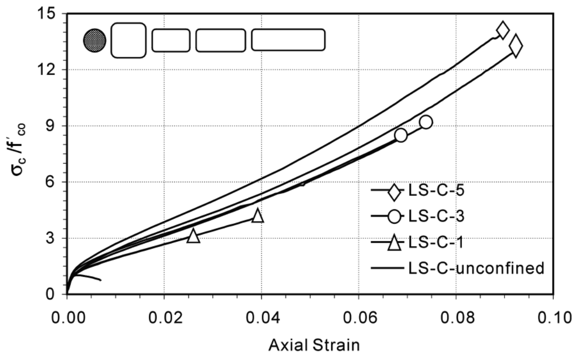

Fig. 4 Axial stress-axial strain relationships for the specimens with circular cross-section

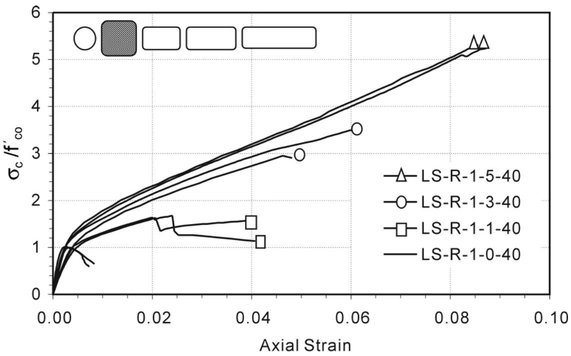

Fig. 5 Axial stress-axial strain relationships for the specimens with square cross-section

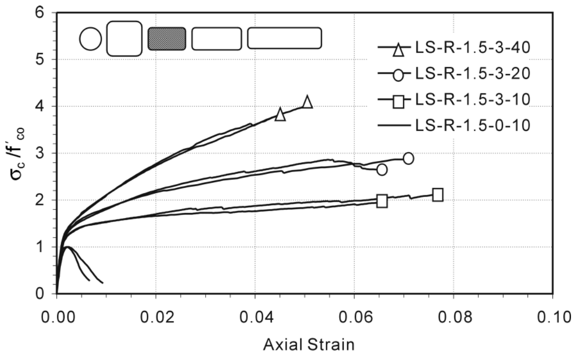

Fig. 6 Axial stress-axial strain relationships for the specimens with rectangular cross-section (depth/width = 1.5)

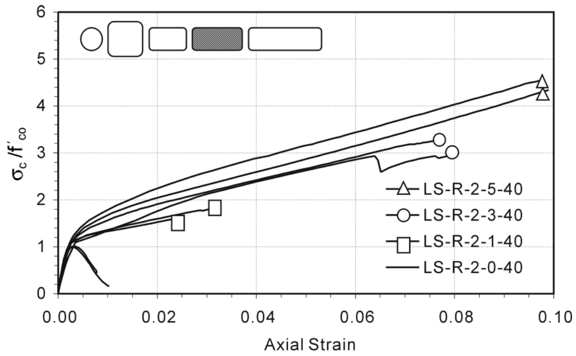

Fig. 7 Axial stress-axial strain relationships for the specimens with rectangular cross-section (depth/width = 2)

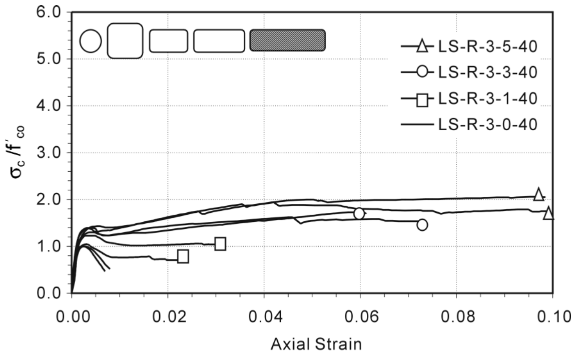

Fig. 8 Axial stress-axial strain relationships for the specimens with rectangular cross-section (depth/width = 3)

expected both the compressive strength and ultimate axial strain increase significantly with an increase of the thickness of the CFRP jacket, Tables 3 and 4. Mirmiran *et al.* (1998) have reported that for square cross-sections the effect of jacket thickness on the behavior was minimal. However,

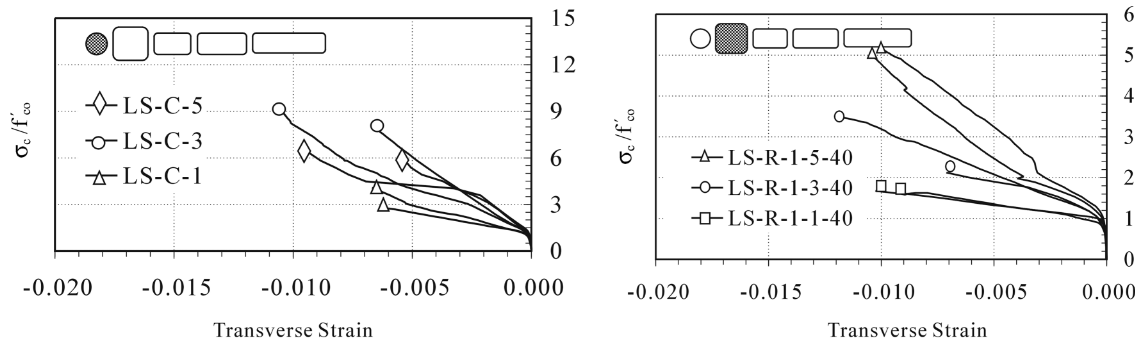

Fig. 9 Axial stress-transverse strain relationships for specimens with circular and square cross-sections

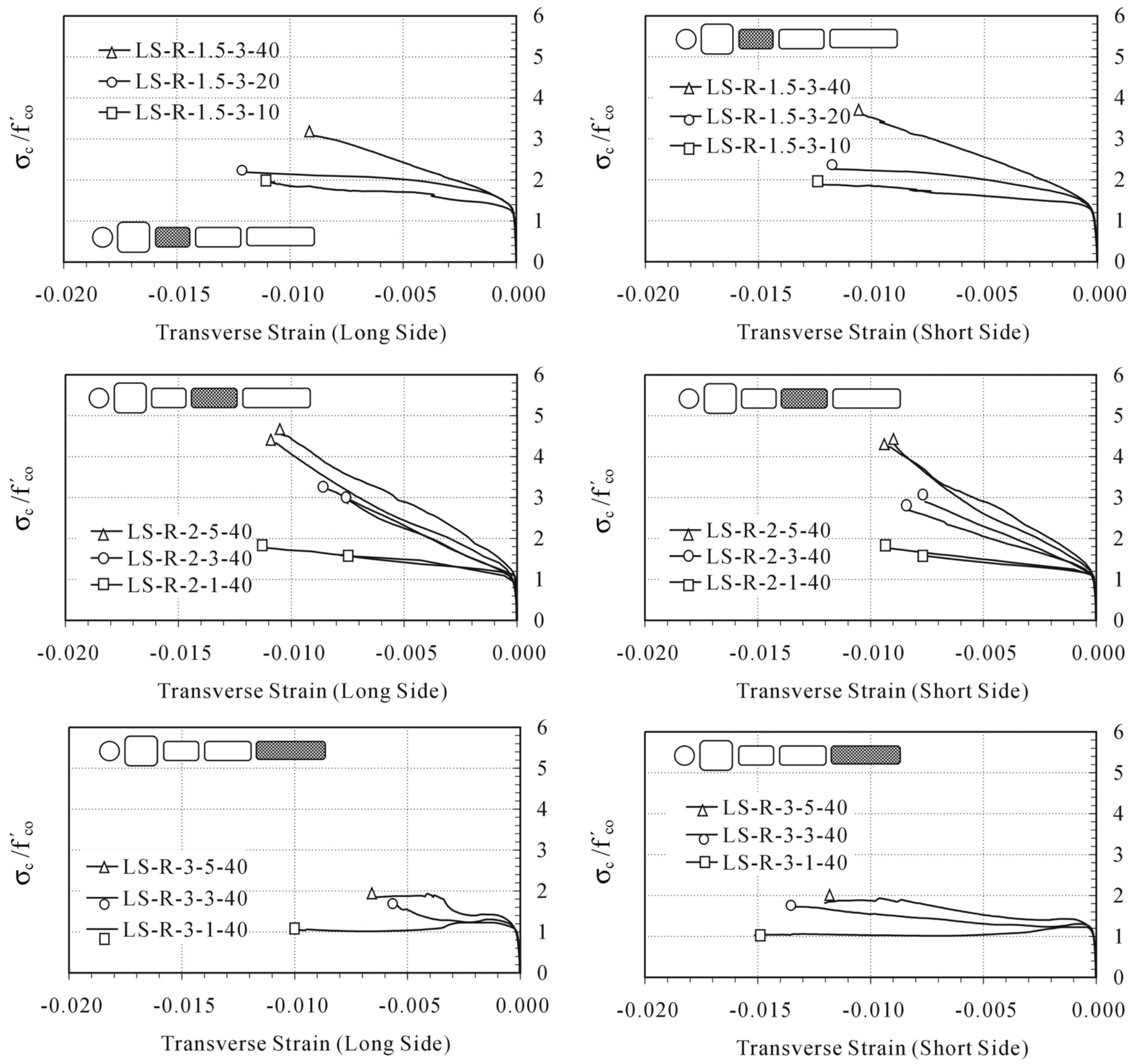

Fig. 10 Axial stress-transverse strain relationships for specimens with rectangular cross-sections

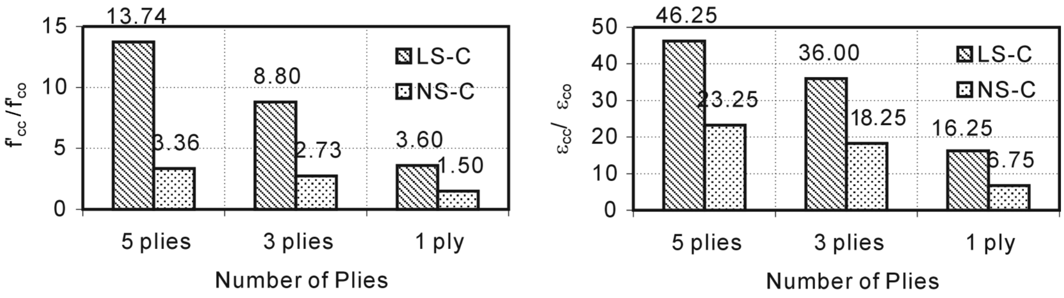

Fig. 11 Enhancements in compressive strength and ultimate axial strain for specimens with circular cross-section for low and normal strength concrete

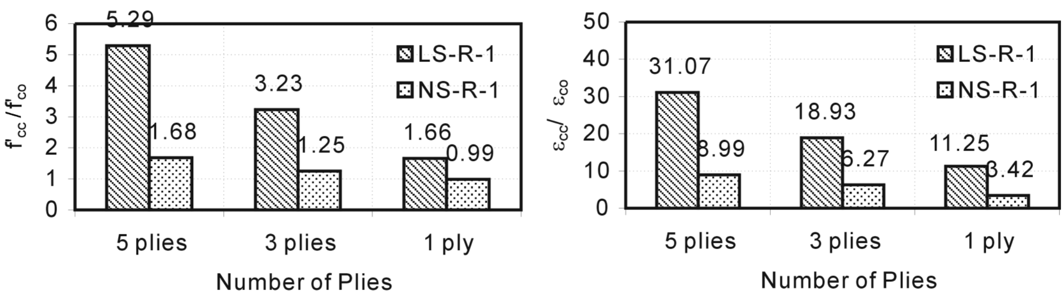

Fig. 12 Enhancements in compressive strength and ultimate axial strain for specimens with rectangular cross-section (depth/width = 1) for low and normal strength concrete

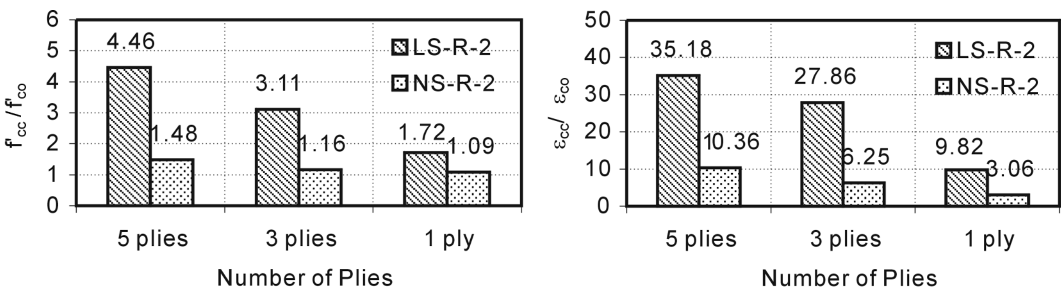

Fig. 13 Enhancements in compressive strength and ultimate axial strain for specimens with rectangular cross-section (depth/width = 2) for low and normal strength concrete

as shown by the test results obtained in this study, when the corners of the rectangular cross-sections are rounded adequately, significantly improved behavior is possible with increasing jacket thickness even for the specimens with relatively larger cross-sectional areas than those tested by Mirmiran *et al.* (1998). Although significant enhancement in strength and deformability was observed for almost all of the CFRP jacketed specimens, the Specimens LS-R-3-1-40a and LS-R-3-1-40b experienced enhancement only in deformability. This can be explained with relatively lower effective transverse confinement pressure provided by CFRP sheets due to relatively larger cross-sectional dimensions, higher ratio of depth to width and thinner jacket thickness. It should also be noted that for all specimens, enhancement in ultimate axial strain was more pronounced than the enhancement in compressive strength.

The measured ultimate transverse strains at failure are generally around 0.009 and 0.0130 independent of the thickness of the CFRP jacket. As may be expected, these values are below the ultimate tensile strain of CFRP composite sheets provided by the manufacturer. The difference may be attributed to the multiaxial state of the stresses, the difference in the difficulty level of the processes of making flat coupons and circular, square or rectangular shaped jackets and possible stress concentrations in CFRP sheets due to cracks and crushing of the damaged concrete. Xiao and Wu (2000) and Fam and Rizkalla (2001) also explained this phenomenon in a similar way.

In Figs. 14, 15 and 16, the relationships between axial strain and normalized dissipated energy are presented for specimens with low (f'_{co} : 6~7 MPa) and normal (f'_{co} : 30~35 MPa) unconfined concrete strengths. In these figures NS and LS represent normal and low strength concrete, respectively. The axial strain-normalized dissipated energy relationships for specimens with normal unconfined concrete strength are taken from the study carried out by Ilki and Kumbasar (2003). As seen in these figures, the increase in compressive strength and ultimate axial strain provided significant enhancement in energy dissipation characteristics for CFRP jacketed specimens. The normalized dissipated energy amounts are almost equal for similar specimens jacketed with different thickness of CFRP sheets at certain levels of axial strains. However, since the specimens with thicker jackets can exhibit relatively higher axial strains, the cumulative energy dissipated by these specimens are significantly higher. The enhancement in energy dissipation for the specimens with low unconfined concrete strength is more remarkable than that of CFRP jacketed specimens of normal strength unconfined concrete. It should be noted that the dissipated energy amounts were calculated as the areas under axial stress-axial strain relationships at certain levels of axial strains. After the areas were calculated, for normalization, all the energy dissipation values were divided by the maximum energy dissipation value.

In Fig. 17, the relationships between tangential Poisson ratios and axial strains are presented for different specimens with circular, square and rectangular cross-section wrapped with 1, 3 and 5 plies of CFRP composite sheets. As seen in this figure, the behavior is significantly different than the behavior of equivalent specimens with normal strength unconfined concrete (f'_{co} : 30~35 MPa), Fig. 18 (Ilki and Kumbasar 2003). In Fig. 18, the first two characters of the names of the specimens, NS stand for normal strength and the names given in parenthesis refer to the original names of these

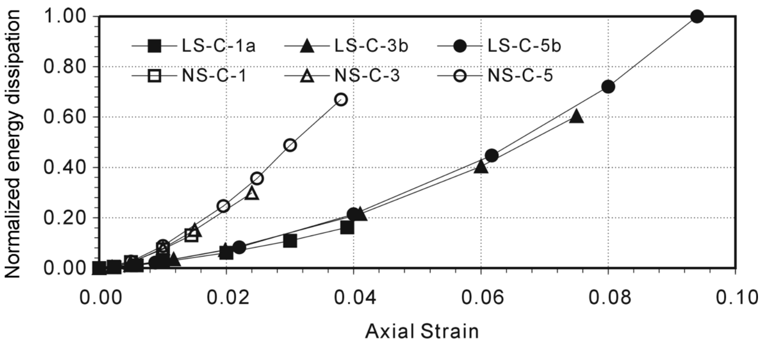

Fig. 14 Axial strain versus dissipated normalized energy relationships for the specimens with circular cross-section for low and normal strength concrete

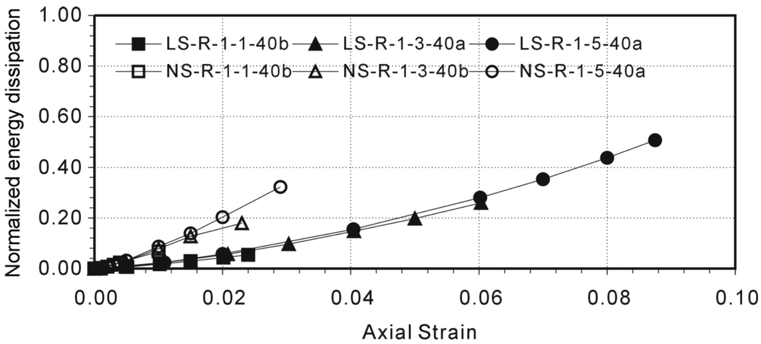

Fig. 15 Axial strain versus dissipated normalized energy relationships for the specimens with rectangular cross-section (depth/width = 1) for low and normal strength concrete

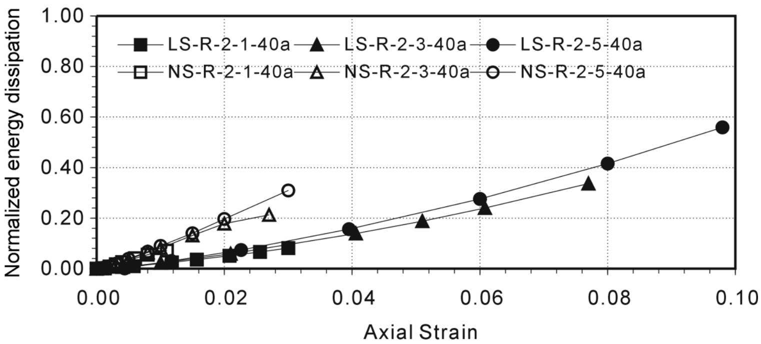

Fig. 16 Axial strain versus dissipated normalized energy relationships for the specimens with rectangular cross-section (depth/width = 2) for low and normal strength concrete

specimens in the study reported by Ilki and Kumbasar (2003). Although for the specimens with normal unconfined concrete strength, there is a sharp increase in tangential Poisson ratio due to microcracking between the axial strain level of 0.002 and 0.003, for specimens with low unconfined concrete strength the increase in tangential Poisson ratio is more gradual than that of the specimens with normal unconfined concrete strength. This is probably due to larger amount of air voids in low strength concrete, which results with more gradual lateral expansion under axial stresses. Then as a result of confinement provided by CFRP jacket, tangential Poisson ratio decreases with the increase in axial strain. As also stated by Wang and Restrepo (2001), it was generally observed that, the thicker jacket results in lower values of tangential Poisson ratio. For the rectangular specimens with the cross-section aspect ratio of 1.5 with different corner radii, it was difficult to determine the effect of corner radii on the tangential Poisson ratio-axial strain relationship, because the specimens with 10 and 40 mm corner radii behaved in a similar manner, while the specimens with 20 mm corner radii experienced much higher tangential Poisson ratio both on long and short sides at axial strains around 0.015~0.025. It is worth noting that although the transverse strain gages on this specimen were out of order at around the axial strain value of 0.02~0.03 while the measured transverse strains were around 0.012, the specimen did not fail until the axial strain level of 0.071. It should also be noted that, during determination of Poisson ratio, it is assumed that there is no slip between concrete and CFRP sheets.

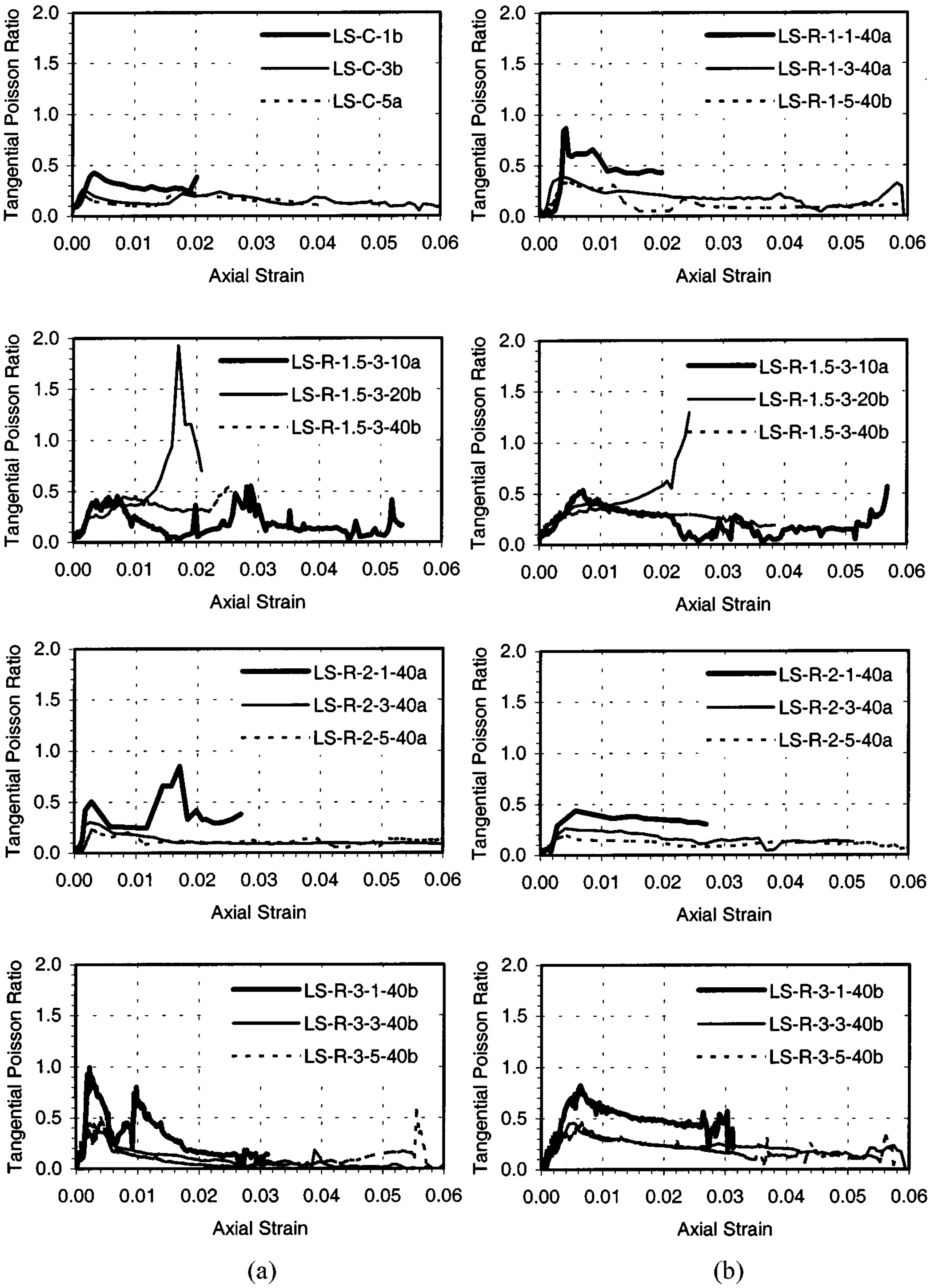

Fig. 17 Tangential Poisson ratios versus average axial strains, (a) long side, (b) short side for rectangular specimens

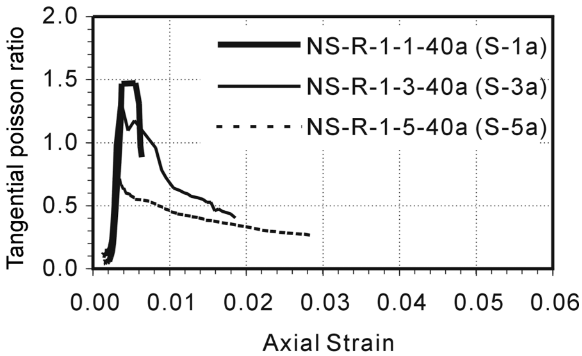

Fig. 18 Tangential Poisson ratios versus average axial strains for the specimens with unconfined concrete strength around 30 MPa (Ilki and Kumbasar 2003)

For specimens with the cross-section aspect ratio of 3, around axial strain of 0.003, the resisted axial stress decreased to different extents as a function of the thickness of the CFRP jacket, Fig. 8. This is probably because CFRP composite sheets, particularly on the long sides of the specimens, could not provide effective confinement until larger lateral deformations, because of their very low flexural stiffness. When axial deformations, and consequently lateral deformations, increase enough to maintain the contact between CFRP composite jacket and concrete, the resisted axial stress began to increase as a result of confinement provided by CFRP composite jacket. Consequently, the enhancement in the compressive strength and the sensitivity of the confinement effects to the thickness of CFRP jacket were relatively lower. This phenomenon was previously observed by Rochette and Labossiere (2000) and Ilki and Kumbasar (2003) too.

The effect of corner radius on the compressive strength and the ultimate axial strain can be seen in Table 4. In this table, it can be seen that while the increase in corner radius resulted with an increase in compressive strength, the ultimate axial strains decreased. The increase in compressive strength can be explained with a more uniform lateral confining pressure state and larger effectively confined area obtained as a consequence of larger corner radius. In contrast to experimental results of Rochette and Labossiere (2000), the ultimate axial strains decreased with increasing corner radius.

As none of the specimens failed because of inadequate overlap length, it can be concluded that overlap length of 150 mm is convenient for the specimens tested in this study. It should be noted that the position of the overlap was on the flat portions of the specimens with rectangular cross-section. Rochette and Labossiere (2000) have observed that an overlap of 100 mm was sufficient for the cylinders of 150 × 300 mm and rectangular specimens of 152 × 203 × 500 mm and 152 × 152 × 500 mm.

The changes of the coordinates of the predetermined points on the surface of the specimens were measured photogrammetrically at each step of the loading in three dimensions. The horizontal and vertical grids formed by these points are shown in Fig. 19. The axial deformations measured on vertical grids in the gage length of 450 mm and the transverse strains measured on horizontal grids in the gage length of 125 mm for the Specimen LS-R-1-5-40b are presented in Fig. 20. As seen in this figure, both axial strains on different vertical grids and transverse strains on different horizontal grids do not show significantly different behavior. The differences between the curves do not follow

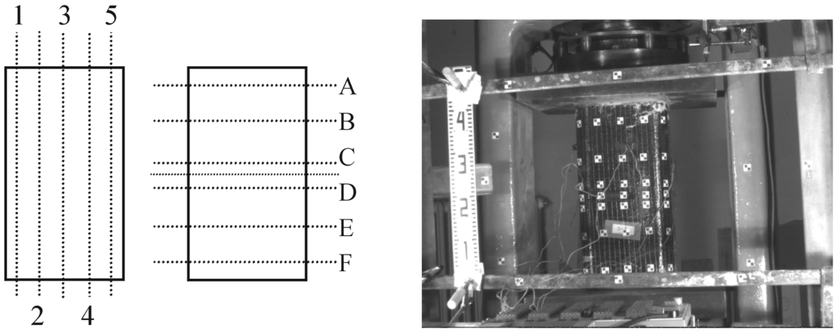

Fig. 19 The horizontal and vertical grids for the photogrammetric measurements

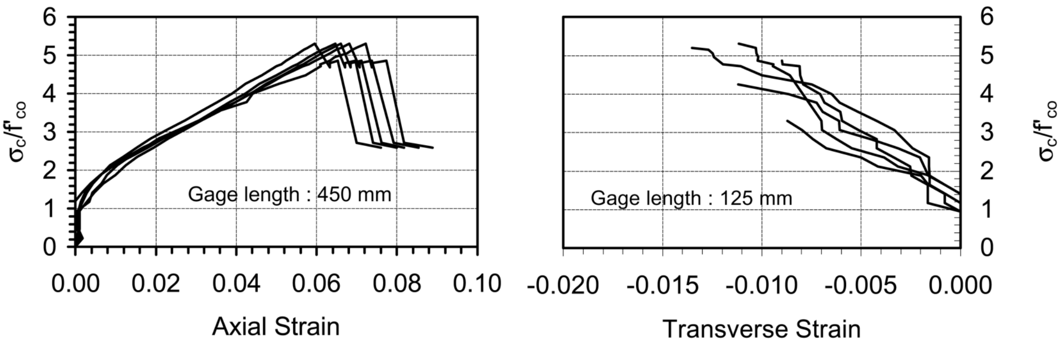

Fig. 20 Distribution of axial and transverse strains for the Specimen LS-R-1-5-40b

any specific trend. A comparison between the average axial strains determined by using displacement transducers and by photogrammetric measurements are presented in Fig. 21, together with the appearance of failure of the Specimen LS-R-1-5-40b. In this figure the gage length considered for the conventional measurement performed by displacement transducers was 500 mm, while 450 and 200 mm gage lengths were considered for photogrammetric measurements. The difference between the measurement performed by displacement transducers in the gage length of 500 mm and the photogrammetric measurement in the gage length of 450 mm may be attributed to the relatively higher axial deformations of the specimen at the top and bottom parts, which are close to the loading platens. The difference between the axial deformations obtained by photogrammetric measurements in the gage lengths of 200 and 450 mm may be attributed to the relatively higher damage of the specimen around the midheight as it can be seen in Fig. 21. Comparisons of the strain gage measurements and photogrammetric measurements for axial and transverse strains are presented in Fig. 22. The gage lengths where the average axial and transverse strains were determined are also indicated in this figure. As seen both axial and transverse strains determined by using photogrammetric measurement technique are very close to those determined by the strain gages. However, it should be noted that since the readability of the strain gages are limited, by using photogrammetric measurement technique much higher strain values can be measured. This is particularly important when relatively higher levels of strains are dealt with, like the case of concrete confined with FRP sheets.

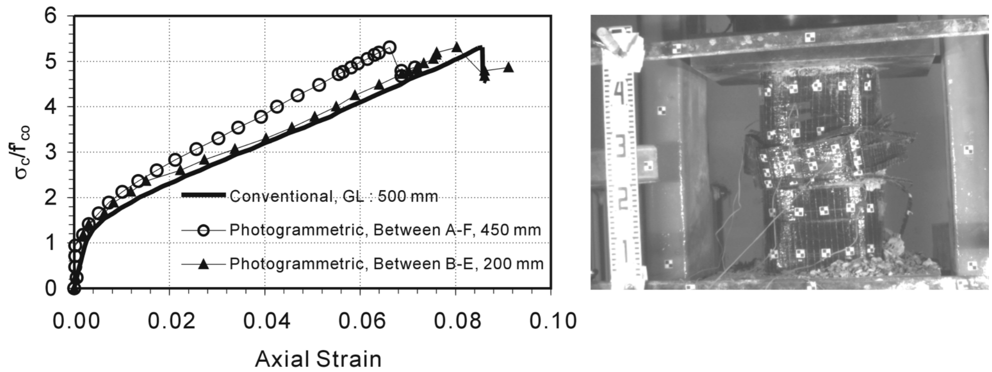

Fig. 21 Effect of the gage length on the axial strains for LS-R-1-5-40b and failure of the specimen

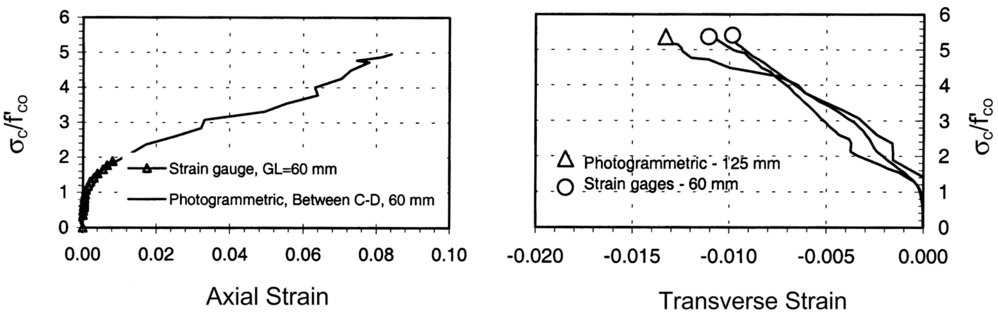

(a) (b)

Fig. 22 Comparison of (a) axial, (b) transverse strains determined by the strain gages and by the photogrammetric measurements

The typical appearances of the cross-sections of the specimens after and before testing are given in Fig. 23. As also observed by other researchers, the failures were due to sudden fracture of CFRP sheets at much higher axial strain levels with respect to unconfined concrete, (Rochette and Labossiere 2000, Chaallal *et al.* 2003). The fractures of CFRP sheets were generally around the corners for the specimens with rectangular cross-sections. It should be noted that the corners of these specimens were rounded with the radii given in Table 4. No dilamination of the fiber sheets from the concrete were observed throughout the tests. For some of the specimens the breakage of the CFRP sheets were observed on full height of the specimens, while for some other specimens the breakages were only a portion of the full height in length irrespective of the provided jacket thickness. The appearances of the failed specimens with different cross-sectional shapes in elevation are presented in Fig. 24. As seen in this figure, although no special measure was taken to prevent local failure at the end portions of the specimens, no premature local failure was observed around the end portions of the specimens. It should also be noted that for the specimens with the cross-sectional dimensions of 150 mm × 450 mm, the ratio of the cross section depth to the specimen height was only 1.11. Normally this ratio is preferred to be higher than or equal to 2 to minimize the effects of friction between the loading platen and the specimen. However, the geometry of the loading system did not permit testing specimens higher than 500 mm. Consequently, it should be

(a) (b)

Fig. 23 (a) LS-R-1.5-3-10a (after test) - LS-R-1.5-3-10b (before test) and (b) LS-R-3-5-40a (after test) - LS-R-3-5-40b (before test)

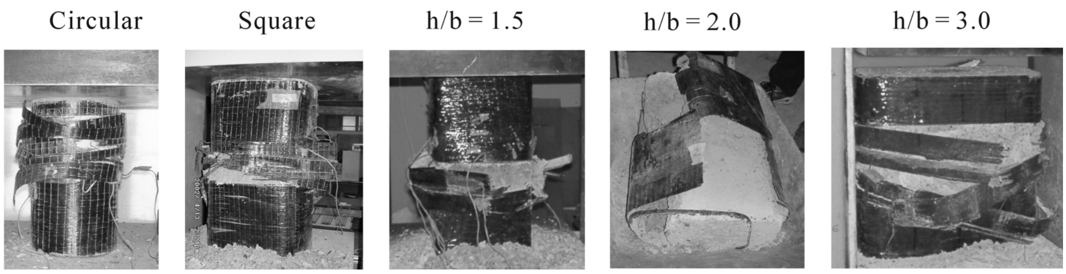

Fig. 24 Typical damages of specimens with circular and rectangular cross-sections of depth/width ratios (h/b) of 1.0, 1.5, 2.0 and 3.0

stated that the additional confinement provided by the friction between the loading platen and the specimen might have caused an artificial enhancement in the performance of these specimens. However, since the ratio of the smaller side of the cross-section to the height is greater than 3 for these specimens, this effect is thought to be of minor importance.

5. Proposed confinement model for low strength concrete members jacketed with CFRP sheets

After the experimental work, it was observed that the axial stress-axial strain relationship of low strength concrete members jacketed with CFRP sheets could be idealized as a bilinear relationship for all different shapes of the cross-sections considered. The model should also reflect a curved transition from the first straight line asymptote with slope E_o to the second line asymptote with slope E_1, Fig. 25. E_o is the initial tangent modulus of CFRP jacketed low strength concrete, which may be assumed to be equal to the initial tangent modulus of unconfined concrete and can be calculated by Eq. (1), and E_1 is the slope of the second straight line and can be calculated using Eq. (2). For the axial stress-axial strain behavior of low strength concrete jacketed by CFRP composite sheets, the four parameter relationship of Richard and Abbot (1975) as modified by

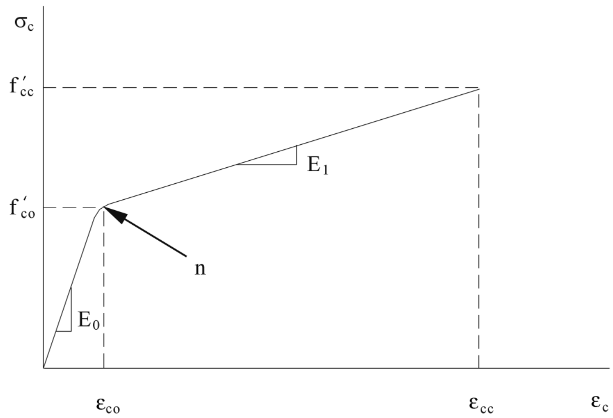

Fig. 25 Axial stress-axial strain model for CFRP jacketed low strength concrete

Samaan *et al.* (1998) is used after minor alterations, Eq. (3). In Eq. (3), σ_c and ε_c are the concrete axial stress and the corresponding axial strain at any stage of loading, and n is the parameter that influences the shape of the transition curve. In this study, n is assumed to have the constant value of 20 for all of the specimens. It should be noted f'_{cc} and ε_{cc} are the confined concrete strength and the ultimate axial strain determined by using Eqs. (5) and (13), respectively.

$$E_0 = 4730\sqrt{f'_{co}} \ (f'_{co} \text{ in MPa}) \tag{1}$$

$$E_1 = \frac{f'_{cc} - f'_{co}}{\varepsilon_{cc} - \varepsilon_{co}} \tag{2}$$

$$\sigma_c = E_1\varepsilon_c + \frac{(E_0 - E_1)\varepsilon_c}{\left[1 + \left(\frac{(E_0 - E_1)\varepsilon_c}{f'_{co}}\right)^n\right]^{\left(\frac{1}{n}\right)}} \tag{3}$$

According to Lam and Teng (2003b), in the case of wrapping around concrete members, FRP ruptures around 60% of its ultimate tensile strain determined by the direct tension tests, (ε_{frp}). Considering this result and the extensive experimental data obtained by the authors for low strength concrete case, ultimate tensile strain of FRP wrapped around concrete members ($\varepsilon_{h,\,rup}$) is assumed to be 70% of the ultimate strain corresponding to tensile strength of FRP, Eq. (4). Consequently, ultimate tensile strength of FRP is considered as 70% of the value determined by direct tension tests. Based on the statistical treatment of the experimental results obtained at the end of this study, it is determined that the compressive strength of FRP confined low strength concrete can be predicted by using Eq. (5) both for the members with circular and non-circular cross-section. In Eq. (5) the maximum effective transverse confinement stress, $f'_{l\max}$, can be obtained by Eq. (6) based on the equilibrium between the resultant transverse compressive force applied on the concrete and the tensile force of the wrapping material.

$$\varepsilon_{h,\,rup} = 0.7\varepsilon_{frp} \tag{4}$$

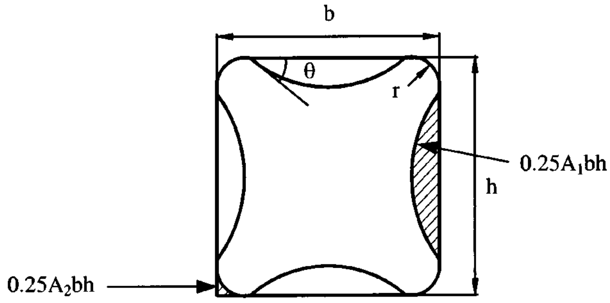

Fig. 26 Effectively confined cross-sectional area

$$f'_{cc} = f'_{co}\left[1 + 2.4\left(\frac{f'_{l\max}}{f'_{co}}\right)^{1.2}\right] \tag{5}$$

$$f'_{l\max} = \frac{\kappa_a \rho_f \varepsilon_{h,rup} E_{frp}}{2} \tag{6}$$

In Eq. (6), κ_a is the efficiency factor that is to be determined based on the section geometry as the ratio of effectively confined cross-sectional area to the gross cross-sectional area, Fig. 26. κ_a, the efficiency factor, can be assumed as 1 for circular cross-sections. For rectangular cross-sections, κ_a can be determined by Eqs. (7), (8) and (9), as also proposed by Wang and Restrepo (2001). In Eq. (6), E_{frp} and ρ_f are the tensile elasticity modulus and ratio of wrapping material to the concrete cross-section, respectively. The ratio of the wrapping material to the concrete cross-section can be determined by Eqs. (10) and (11) for circular and rectangular cross-sections, respectively.

$$\kappa_a = 1 - A_1 - A_2 - \rho \tag{7}$$

$$A_1 = \frac{(b-2r)^2 + (h-2r)^2}{3bh}\tan\theta \tag{8}$$

$$A_2 = \frac{4r^2 - \pi r^2}{bh} \tag{9}$$

$$\rho_f = \frac{4n_f t_f}{D} \tag{10}$$

$$\rho_f = \frac{2n_f t_f(b+h)}{bh} \tag{11}$$

In above equations, ρ is the ratio of cross-sectional area of the longitudinal reinforcement to the cross-sectional area of wrapped member, θ is the arching angle and r is the radius of the member corner. Wang and Restrepo (2001) reported that θ varied between 42 and 47 degrees. In this study, based on the observations on the damaged specimens, θ is assumed as 45 degrees. In Eqs. (10) and (11), t_f and n_f are the effective thickness and the number of plies of wrapping material, D is the diameter of the circular cross-section, and b and h are the width and depth of the rectangular member to be wrapped. As also stated by Lam and Teng (2003b) for ACI (2002) model, the equivalent circular column is defined as a column, which has the same volumetric ratio of FRP as that of the original rectangular column. The equivalent circular column diameter can be obtained by Eq. (12).

$$D = \frac{2bh}{b+h} \tag{12}$$

After statistical evaluation of the experimental data, the equation given below is proposed for the ultimate axial strain of FRP composite jacketed low strength concrete, Eq. (13).

$$\varepsilon_{cc} = \varepsilon_{co}\left(1 + 20\left(\frac{h}{b}\right)\left(\frac{f'_{l\max}}{f'_{co}}\right)^{0.5}\right) \tag{13}$$

The axial stress-axial strain relationships predicted by the proposed equations for the specimens with circular and rectangular cross-sections tested in this study are presented together with the experimental axial stress-axial strain relationships in Fig. 27. It should be noted that the proposed model is valid, when the ratio of ($f'_{l\max}/f'_{co}$) is higher than 0.3. According to the test results obtained

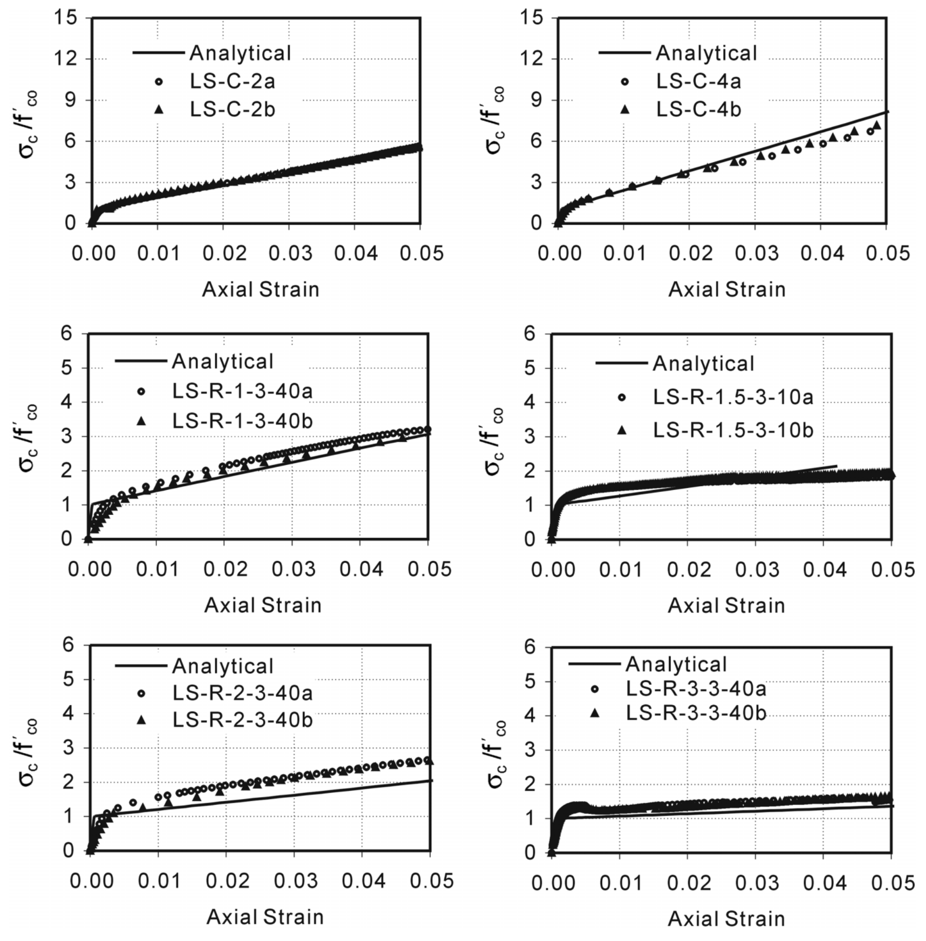

Fig. 27 Comparison of the analytical and the experimental axial stress-axial strain relationships

in this study, the ratio of ($f'_{l\max}/f'_{co}$) higher than 0.3 guarantees an increase in the compressive strength of concrete. This limiting value is reported as 0.07 for normal strength concrete members by Lam and Teng (2003a).

6. Comparison of predicted and measured axial strengths and ultimate strains

The predicted and the measured axial compressive strengths and ultimate axial strains for specimens with circular and rectangular cross-sections are presented in Tables 5 and 6, respectively. As seen in these tables, both the axial compressive strengths and the ultimate axial strains are predicted with a reasonable accuracy for almost all of the specimens tested in this study. The exceptions are the ultimate axial strains of the specimens LS-R-1.5-3-10a and LS-R-1.5-3-10b with the corner radius of 10 mm. The ultimate axial strains of these two specimens are underestimated with a significant difference. For all of the specimens presented in Tables 5 and 6, the average of the ratios of experimental to analytical compressive strengths predicted by Eq. (5) is 1.02 with a standard deviation of 0.11. In these tables, the average and the standard deviation of the ratios of experimental to analytical ultimate axial strains predicted by Eq. (13) are 0.99 and 0.23, respectively. The comparison of the predicted and the measured axial strengths and ultimate strains are also presented in Tables 5 and 6.

It should be noted that the verification of the proposed equations and the stress-strain relationship could be done only for the specimens tested by the authors themselves due to absence of experimental data on the CFRP jacketed low strength concrete. It is also noteworthy to mention that the available equations proposed for the axial strength and ultimate axial strain of normal strength concrete members cannot predict the compressive strength and the ultimate axial strain values accurately for CFRP jacketed low strength concrete members. Since almost all of the available

Table 5 Comparison of the experimental and the analytical results for the specimens with circular cross-section

Specimen	h/b	f'_{co} (MPa)	Fiber Layer	f'_{cc} (MPa) (exp.)	ε_{cc} (lvdt) (exp.)	ρ_f	$f'_{l\max}$ (MPa)	$f'_{l\max}/f'_{co}$	f'_{cc} (MPa) (analytical)	5/10	ε_{cc} (analytical)	6/12
(1)	(2)	(3)	(4)	(5)	(6)	(7)	(8)	(9)	(10)	(11)	(12)	(13)
LS-C-1a	1	6.2	1	25.3	0.039	0.00440	5.31	0.86	18.56	1.36	0.039	1.00
LS-C-1b	1	6.2	1	19.4	0.026	0.00440	5.31	0.86	18.56	1.05	0.039	0.67
LS-C-2a	1	6.2	2	41.9	0.059	0.00880	10.63	1.71	34.60	1.21	0.054	1.09
LS-C-2b	1	6.2	2	40.0	0.059	0.00880	10.63	1.71	34.60	1.16	0.054	1.09
LS-C-3a	1	6.2	3	52.2	0.069	0.01320	15.94	2.57	52.40	1.00	0.066	1.04
LS-C-3b	1	6.2	3	56.9	0.075	0.01320	15.94	2.57	52.40	1.09	0.066	1.13
LS-C-4a	1	6.2	4	76.6	0.085	0.01760	21.25	3.43	71.45	1.07	0.076	1.12
LS-C-4b	1	6.2	4	69.7	0.076	0.01760	21.25	3.43	71.45	0.98	0.076	1.00
LS-C-5a	1	6.2	5	87.7	0.091	0.02200	26.57	4.28	91.49	0.96	0.085	1.07
LS-C-5b	1	6.2	5	82.7	0.094	0.02200	26.57	4.28	91.49	0.90	0.085	1.11
LS-C-6a	1	6.2	6	108.3	0.104	0.02640	31.88	5.14	112.35	0.96	0.093	1.12
LS-C-6b	1	6.2	6	103.3	0.096	0.02640	31.88	5.14	112.35	0.92	0.093	1.04

Table 6 Comparison of the experimental and the analytical results for the specimens with rectangular cross-section

Specimen	h/b	f'_{co} (MPa)	Fiber Layer	f'_{cc} (MPa) (exp.)	ε_{cc} (lvdt) (exp.)	ρ_f	$f'_{l\max}$ (MPa)	$f'_{l\max}/f'_{co}$	f'_{cc} (MPa) (analytical)	5/10	ε_{cc} (analytical)	6/12
(1)	(2)	(3)	(4)	(5)	(6)	(7)	(8)	(9)	(10)	(11)	(12)	(13)
LS-R-1-1-40a	1	6.8	1	11.1	0.039	0.00264	2.14	0.32	10.88	1.02	0.034	1.14
LS-R-1-1-40b	1	6.8	1	11.4	0.024	0.00264	2.14	0.32	10.88	1.05	0.034	0.70
LS-R-1-3-40a	1	6.8	3	23.8	0.060	0.00792	6.43	0.95	22.05	1.08	0.057	1.05
LS-R-1-3-40b	1	6.8	3	20.1	0.046	0.00792	6.43	0.95	22.05	0.91	0.057	0.80
LS-R-1-5-40a	1	6.8	5	35.8	0.088	0.0132	10.71	1.58	34.95	1.02	0.073	1.20
LS-R-1-5-40b	1	6.8	5	36.1	0.086	0.0132	10.71	1.58	34.95	1.03	0.073	1.18
LS-R-1.5-3-10a	1.5	9.5	3	18.6	0.066	0.011	5.53	0.58	21.40	0.87	0.048	1.38
LS-R-1.5-3-10b	1.5	9.5	3	20.2	0.076	0.011	5.53	0.58	21.40	0.94	0.048	1.59
LS-R-1.5-3-20a	1.5	9.5	3	27.1	0.056	0.011	7.07	0.74	25.48	1.06	0.054	1.04
LS-R-1.5-3-20b	1.5	9.5	3	27.3	0.071	0.011	7.07	0.74	25.48	1.07	0.054	1.32
LS-R-1.5-3-40a	1.5	9.5	3	37.9	0.050	0.011	9.34	0.98	31.83	1.19	0.061	0.81
LS-R-1.5-3-40b	1.5	9.5	3	36.2	0.045	0.011	9.34	0.98	31.83	1.14	0.061	0.73
LS-R-2-3-40a	2	7.2	3	23.6	0.077	0.0099	6.87	0.95	23.54	1.00	0.112	0.69
LS-R-2-3-40b	2	7.2	3	21.1	0.079	0.0099	6.87	0.95	23.54	0.90	0.112	0.70
LS-R-2-5-40a	2	7.2	5	32.8	0.098	0.0165	11.46	1.59	37.37	0.88	0.144	0.68
LS-R-2-5-40b	2	7.2	5	31.3	0.099	0.0165	11.46	1.59	37.37	0.84	0.144	0.69
LS-R-3-3-40a	3	9.8	3	15.1	0.072	0.0088	2.98	0.30	15.43	0.98	0.082	0.88
LS-R-3-3-40b	3	9.8	3	16.6	0.061	0.0088	2.98	0.30	15.43	1.08	0.082	0.75
LS-R-3-5-40a	3	9.8	5	20.1	0.098	0.0147	4.96	0.51	20.19	1.00	0.105	0.93
LS-R-3-5-40b	3	9.8	5	17.1	0.099	0.0147	4.96	0.51	20.19	0.85	0.105	0.94

models were proposed based on the axial tests of concrete members having the concrete strengths around 30 MPa or higher, this consequence seems reasonable.

7. Conclusions

The following conclusions are derived at the end of the experimental work carried on 14 specimens with circular cross-section, and 32 specimens with rectangular cross-sections of depth to width ratios of 1, 1.5, 2 and 3.

CFRP composite sheet jacketing of low strength concrete members with circular, square and rectangular ($h/b = 1.5$, 2 and 3) cross-sections significantly improves the compressive behavior in terms of strength and deformability. As a result of these improvements, significant enhancement can be obtained for energy dissipation capacities of these members. It should be emphasized that for significant enhancement in compressive strength of the rectangular specimens, corners should be rounded adequately. Since the efficiently confined cross-sectional areas are relatively higher in the case of specimens with circular cross-sections with respect to the similar specimens with rectangular cross-sections, the enhancement in compressive strength and deformability is more significant for the same thickness of CFRP jacket. However, provided that ($f'_{l\max}/f'_{co}$) values are the same, similar enhancement in compressive strength and deformability is possible for low strength concrete members with circular and rectangular cross-sections. It is also noteworthy to mention that the efficiency of the external CFRP jacket on the compressive strength, and particularly on the deformability is much more pronounced when the unconfined concrete compressive strength is relatively low.

Simple analytical expressions are proposed for the compressive strength and ultimate axial strain of the CFRP jacketed low strength concrete members of circular, square and rectangular cross-sections. The analytical results obtained by these simple expressions are in good agreement with the experimental data presented in this study. It should be noted that the validity of these expressions is limited within the range of the variables considered in this study.

8. Further study

In many cases the problems of low strength concrete and inadequate transverse reinforcement exist together for the existing buildings. Consequently, the positive contribution of existing transverse reinforcement to the confinement of the structural members is often negligible. However, inadequate transverse reinforcement brings the problem of longitudinal bar buckling, which is not taken into account in this study as well as most of other available studies. For further study, it is planned to carry out tests on similar specimens with longitudinal reinforcement to be able to observe the contribution of external CFRP jacketing to the buckling problem of longitudinal reinforcing bars.

Acknowledgments

The experimental study is financially supported by the Turkish Earthquake Foundation (Project No: 01-AP-118) and Degussa-Yapkim Construction Chemicals Company. The contributions of Prof.Dr. M. Orhan Altan and Dr. Bahadir Ergun during photogrammetrical measurements and Mr. Cem Demir during experimental work are also acknowledged.

References

Ahmad, S.H. and Shah, S.P. (1985), “Behavior of hoop confined concrete under high strain rates”, *J. the American Concrete Institute*, **82**, 634-647.

American Concrete Institute (2002), “Guide for the design and construction of externally bonded FRP systems for strengthening concrete structures”, ACI Committee 440, Technical Committee Document 440.2R-02.

Becque, J., Patnaik, A.K. and Rizkalla, S.H. (2003), “Analytical models for concrete confined with FRP tubes”, *J. Compos. Const*., **7**(1), 31-38.

Campione, G. and Miraglia, N. (2003), “Strength and strain capacities of concrete compression members reinforced with FRP”, *Cement & Concrete Composites*, **25**, 31-41.

Chaallal, O., Shahawy, M. and Hassan, M. (2003), “Performance of axially loaded short rectangular columns strengthened with carbon fiber-reinforced polymer wrapping”, *J. Compos. Const.*, **7**(3), 200-208.

De Lorenzis, L. and Tepfers, R. (2003), “Comparative study of models on confinement of concrete cylinders with fiber-reinforced polymer composites”, *J. Compos. Const.*, **7**(3), 219-237.

Demers, M. and Neale, K.W. (1994), “Strengthening of concrete columns with unidirectional composite sheets”, Development in Short and Medium Span Bridge Engineering '94, *Proc., 4th Int. Conf. on Short and Medium Bridges*, A.A. Mufti, B. Bakht, and L.G. Jaeger, eds., Canadian Society for Civil Engineering, Montreal, 895-905.

Demers, M. and Neale, K.W. (1999), “Confinement of reinforced concrete columns with fibre-reinforced composite sheets-an experimental study”, *Can. J. Civ. Eng.*, **26**(2), 226-241.

Fam, A.Z. and Rizkalla, S.H. (2001), “Confinement model for axially loaded concrete confined by circular fiber-reinforced polymer tubes”, *ACI Struct. J.*, **98**(4), 451-461.

Fardis, M.N. and Khalili, H. (1982), “FRP-encased concrete as a structural material”, *Magazine of Concrete Research*, **34**(121), 191-202.

Fukuyama, H. and Sugano, S. (2000), “Japanese seismic rehabilitation of concrete buildings after the Hyogoken-Nanbu earthquake”, *Cement & Concrete Composites*, **22**, 59-79.

Fyfe, E.R. (1996), “Column seismic retrofitting using high-strength fiber jackets”, *Seismic Rehabilitation of Concrete Structures*, **ACI SP-160**, 161-168.

Guadagnini, M., Pilakoutas, K. and Waldron, P. (2001), “An overview of the European research on FRPs and their applications”, *Proc. of Int. Conf. on FRP Composites in Civil Engineering*, Hong Kong, 1699-1706.

Harmon, T.G. and Slattery, K.T. (1992), “Advanced composite confinement of concrete”, *Proc., 1st Int. Conf. on Advanced Composite Materials in Bridges and Structures*, K.W. Neale and P. Labossiere, eds., Canadian Society for Civil Engineering, Sherbrooke, Canada, 299-306.

Hoshikuma, J., Kawashima, K., Nagaya, K. and Taylor, A.W. (1997), “Stress-strain model for confined reinforced concrete in bridge piers”, *J. Struct. Eng.*, ASCE, **123**(5), 624-633.

Igarashi, S. (1999), “Recommendations on minimizing earthquake damage in big cities in Turkey”, *Proc., Int. Conf. on the Kocaeli Earthquake*, Istanbul, Turkey, 271-286.

Ilki, A., Ozdemir, P. and Fukuta, T. (1997), *Confinement Effect of Reinforced Concrete Columns with Circular Cross-Section*, BRI Research Paper, 143, Building Research Institute, Tsukuba.

Ilki, A. and Kumbasar, N. (2002), “Behavior of damaged and undamaged concrete strengthened by carbon fiber composite sheets”, *Struct. Eng. Mech.*, **13**(1), 75-90.

Ilki, A. and Kumbasar, N. (2003), “Compressive behaviour of carbon fibre composite jacketed concrete with circular and non-circular cross-sections”, *J. Earthq. Eng.*, **7**(3), 381-406.

Karbhari, V.M. and Gao, Y. (1997), “Composite jacketed concrete under uniaxial compression-verification of simple design equations”, *J. Materials in Civil Engineering*, ASCE, **9**(4), 185-193.

Kent, D.C. and Park, R. (1971), “Flexural members with confined concrete”, *J. Struct. Div.*, ASCE, **97**(ST7), 1969-1990.

Lam, L. and Teng, J.G. (2002), “Strength models for fiber-reinforced plastic-confined concrete”, *J. Struct. Eng.*, ASCE, **128**(5), 612-623.

Lam, L. and Teng, J.G. (2003a), “Design-oriented stress-strain model for FRP-confined concrete”, *Construction and Building Materials*, **17**, 471-489.

Lam, L. and Teng, J.G. (2003b), “Design-oriented stress-strain model for FRP-confined concrete in rectangular columns”, *Journal of Reinforced Plastics and Composites*, **22**(13), 1149-1186.

Maalej, M., Tanwongsval, S. and Paramasivam, P. (2003), “Modelling of rectangular RC columns strengthened with FRP”, *Cement & Concrete Composites*, **25**, 263-276.

Mander, J.B., Priestley, M.J.N. and Park, R. (1988a), “Observed stress-strain behaviour of confined concrete”, *J. Struct. Div.*, ASCE, **114**(8), 1827-1849.

Mander, J.B., Priestley, M.J.N. and Park, R. (1988b), “Theoretical stress-strain model for confined concrete”, *J. Struct. Div.*, ASCE, **114**(8), 1804-1826.

Mbrace Product Catalogues, (2000), YKS Construction Chemicals, Turkey.

Mirmiran, A. and Shahawy, M. (1997), “Behavior of concrete columns confined by fiber composites”, *J. Struct. Eng.*, ASCE, **123**(5), 583-590.

Mirmiran, A., Shahawy, M., Samaan, M., El Echary, H., Mastrapa, J.C. and Pico, O. (1998), “Effect of column parameters on FRP-confined concrete”, *J. Comp. Const.*, ASCE, **2**(4), 175-185.

Mugurama, H. and Watanabe, F. (1990), "Ductility improvement of high-strength concrete columns with lateral confinement", *in ACI Spec. Publ.*, **SP-121-4**, Am. Conc. Inst., Detroit, Mich., 47-60.

Mugurama, H., Watanabe, F., Iwashimizu, T. and Mitsueda, R. (1983), "Ductility improvement of high strength concrete by lateral confinement", *Transactions of Japan Concrete Institute*, **5**, 403-410.

Nanni, A. and Bradford, N.M. (1995), "FRP jacketed concrete under uniaxial compression", *Constr. Build. Mater.*, **9**(2), 115-124.

Park, R., Priestley, M.J.N. and Gill, W.D. (1982), "Ductility of square-confined concrete columns", *J. Struct. Div.*, ASCE, **108**(ST4), 929-950.

Priestley, M.J.N., Park, R. and Potangaroa, R.T. (1981), "Ductility of spirally confined columns", *J. Struct. Div.*, ASCE, **107**(ST1), 181-202.

Richard, R.M. and Abbot, B.J. (1975), "Versatile elastic-plastic stress-strain formula", *J. Eng. Mech.*, ASCE, **101**(4), 511-515.

Rochette, P. and Labossiere, P. (2000), "Axial testing of rectangular column models confined with composites", *J. Comp. Const.*, ASCE, **4**(3), 129-136.

Saadatmanesh, H., Ehsani, M.R. and Li, M.W. (1994), "Strength and ductility of concrete columns externally reinforced with fiber composite straps", *ACI Struct. J.*, **91**(4), 434-447.

Saafi, M., Toutanji, H. and Li, Z. (1999), "Behavior of concrete columns confined with fiber reinforced polymer tubes", *ACI Materials J.*, **96**(4), 500-509.

Saatcioglu, M. and Razvi, S.R. (1992), "Strength and ductility of confined concrete", *J. Struct. Div.*, ASCE, **118**(6), 1590-1607.

Saatcioglu, M., Salamat, A.H. and Razvi, S.R. (1995), "Confined columns under eccentric loading", *J. Struct. Eng.*, ASCE, **121**(11), 1547-1556.

Samaan, M., Mirmiran, A. and Shahawy, M. (1998), "Model of concrete confined by fiber composites", *J. Struct. Eng.*, ASCE, **124**(9), 1025-1031.

Sheikh, S.A. and Uzumeri, S.M. (1982), "Analytical model for concrete confinement in tied columns", *J. Struct. Div.*, ASCE, **108**(ST12), 2703-2722.

Spoelstra, M.R. and Monti, G. (1999), "FRP-confined concrete model", *J. Compos. Const.*, **3**(3), 143-150.

Tan, K.H. (2002), "Strength enhancement of rectangular reinforced concrete columns using fiber-reinforced polymer", *J. Compos. Const.*, **6**(3), 175-183.

Teng, J.G. and Lam, L. (2002), "Compressive behavior of carbon fiber reinforced polymer-confined concrete in elliptical columns", *J. Struct. Eng.*, **128**(12), 1535-1543.

Toutanji, H.A. (1999), "Stress - strain characteristics of concrete columns externally confined with advanced fiber composite sheets", *ACI Materials J.*, **96**(3), 397-404.

Wang, Y.C., Restrepo, J.I. and Park, R. (2000), "Retrofit of reinforced concrete members using advanced composite materials", Research Report 2000-3, Department of Civil Engineering, University of Canterbury, New Zealand.

Wang, Y.C. and Restrepo, J.I. (2001), "Investigation of concentrically loaded reinforced concrete columns confined with glass fiber-reinforced polymer jackets", *ACI Struct. J.*, **98**(3), 377-385.

Xiao, Y. and Wu, H. (2000), "Compressive behaviour of concrete confined by carbon fiber composite jackets", *J. Materials Civil Eng.*, ASCE, **12**(2), 139-146.

Notation

A_1, A_2 : cross-sectional areas which are not confined efficiently
b : width of the cross-section
D : member diameter
E_o : initial tangent modulus
E_1 : slope of the second straight line of the proposed stress-strain relationship
E_{frp} : elasticity modulus of FRP
f'_c : standard cylinder compressive strength
f'_{co} : unconfined concrete compressive strength of the member

f'_{cc} : compressive strength of concrete jacketed with FRP composite sheet
$f'_{l\max}$: maximum effective transverse confinement stress
h : depth of the cross-section
n : parameter for the shape of the transition curve
n_f : number of FRP plies
r : corner radius
t_f : effective thickness of FRP sheets
ε_c : axial concrete strain at any step of loading
ε_{co} : axial strain corresponding to unconfined concrete compressive strength
ε_{cc} : ultimate axial strain for FRP composite sheet jacketed concrete
ε_{ch} : ultimate transverse strain for FRP composite sheet jacketed concrete
ε_{frp} : ultimate tensile strain determined for FRP by the direct tension tests
$\varepsilon_{h,rup}$: ultimate tensile strain of FRP wrapped around concrete members
κ_a : efficiency factor
θ : arching angle (45º)
ρ : ratio of the cross-sectional area of the longitudinal reinforcement to the concrete cross-section area
ρ_f : ratio of the cross-sectional area of FRP jacket to the cross-sectional area of concrete
σ_c : axial concrete stress at any step of loading